# Freezing of mixtures confined in silica nanopores: Experiment and molecular simulation

Benoit Coasne,[1,a)] Joanna Czwartos,[2,3] Malgorzata Sliwinska-Bartkowiak,[2] and Keith E. Gubbins[4]
[1]*Institut Charles Gerhardt Montpellier (UMR 5253), CNRS, Université Montpellier 2, ENSCM, 8 rue de l'Ecole Normale, 34296 Montpellier Cedex 05, France*
[2]*Institute of Physics, Adam Mickiewicz University, Umultowska 85, 61-614 Poznan, Poland*
[3]*Institute of Optoelectronics, Military University of Technology, Kaliskiego 2 Str., 01-489 Warsaw, Poland*
[4]*Department of Chemical and Biomolecular Engineering and Institute for Computational Sciences and Engineering, North Carolina State University, Raleigh, North Carolina 27695-7905, USA*

(Received 19 April 2010; accepted 23 June 2010; published online 24 August 2010)

Freezing of mixtures confined in silica nanopores is investigated by means of experiment and molecular simulation. The experiments consist of differential scanning calorimetry and dielectric relaxation spectroscopy measurements for $CCl_4/C_6H_5Br$ mixtures confined in Vycor having pores with a mean diameter of about $D=4.2$ nm. Molecular simulations consist of grand canonical Monte Carlo simulations combined with the parallel tempering technique for Lennard-Jones Ar/Kr mixtures confined in a silica cylindrical nanopore with a diameter of $D=3.2$ nm. The experimental and molecular simulation data provide a consistent picture of freezing of mixtures in cylindrical silica nanopores having a size smaller than ten times the size of the confined molecules. No sharp change in the properties of the confined mixture occurs upon melting, which suggests that the confined system does not crystallize. In the case of the molecular simulations, this result is confirmed by the fact that except for the contact layer, the percentage of crystal-like atoms is less than 6% (whatever the temperature). The molecular simulations also show that the composition of the mixture is shifted, upon confinement, toward the component having the strongest wall/fluid attraction. © *2010 American Institute of Physics*. [doi:10.1063/1.3464279]

## I. INTRODUCTION

Freezing and melting of fluids or mixtures confined at the nanoscale is relevant to practical applications involving lubrication, adhesion, nanotribology, and fabrication of nanomaterials. For instance, the use of nanoporous solids as templates to obtain nanomaterials such as composites, nanowires, or nanotubes is receiving increasing attention.[1–9] Freezing in porous media has also been widely employed in the characterization of porous materials using the method of thermoporometry.[10] In this method the change in the freezing temperature is related to the pore size through the Gibbs–Thomson equation. From a fundamental point of view, freezing of systems confined in nanopores can be used to estimate the effect of confinement, surface forces, and reduced dimensionality on the thermodynamics and dynamics of fluids.[8,10,11] Upon reducing the width of the confined space to approach the range of the intermolecular forces, significant shifts in the freezing temperature are observed and, in some cases, new surface- or confinement-induced phases occur.[8,10–13] Previous experimental, molecular simulation, and theoretical studies have shown that for simple fluids and pore geometries, the freezing temperature can be described as a function of the reduced pore size $H^*=H/\sigma$ (where $H$ is the pore width and $\sigma$ is the diameter of the adsorbate molecule) and the ratio of the wall/fluid ($wf$) to the fluid/fluid ($ff$) interactions, $\alpha \sim C\rho_w\varepsilon_{wf}/\varepsilon_{ff}$, where $\rho_w$ and $\varepsilon$ are the density of wall atoms and the potential well depth, respectively, and $C$ is a constant that depends on the pore geometry. The freezing temperature $T_f$ is decreased compared to the bulk $T_f^0$ for $\alpha<1$, while it is increased for $\alpha>1$. The magnitude of the shift in the transition temperature depends on $H$, while the appearance of surface- or confinement-induced phases usually depends on a combination of effects from $H$ and $\alpha$ (for a recent review on the effects of confinement and surface forces on freezing, see Ref. 8).

For sufficiently large pores, the shift in the freezing temperature $\Delta T_f$ can be related to the pore width $H^*$ using the Gibbs–Thomson equation that is obtained either by equating the free energies of the confined liquid and solid phases[14] or by determining the temperature at which the chemical potential of the confined solid equals that of the bulk reservoir.[15] In agreement with the Gibbs–Thomson equation, early experiments, which were performed for pores larger than 6–7 nm, showed a linear relation between the in-pore freezing temperature and the inverse pore width. However, the equation fails to predict the freezing temperature for smaller pores due to the breakdown of Gibbs' surface thermodynamics. Differential scanning calorimetry and dielectric relaxation spectrometry for $CCl_4$ confined in controlled porous glasses showed that the Gibbs–Thomson equation fails to describe the shift in freezing temperature for pores smaller than $\sim 15\sigma$ (i.e., ~7.5 nm).[16] Similarly, the equation fails for $CCl_4$ in activated carbon fibers (pore width of 1.1–1.7

[a)]Author to whom correspondence should be addressed. Electronic mail: benoit.coasne@enscm.fr. Tel.: +33467163459. FAX: +33467163470.

 

nm).[17] This breakdown is due to the use in the derivation of the Gibbs–Thomson equation of macroscopic concepts, such as surface tensions (implying an interface separating two bulklike phases), and the failure to account for the strong inhomogeneity of the confined phase. Even when the Gibbs–Thomson equation is expected to apply, its use is usually limited by the unavailability of the surface tensions involved.

A qualitative understanding of the effects of confinement on freezing temperature can be obtained from the following reasoning, which does not rest on macroscopic arguments concerning surface tension. If we assume that the fluid molecules can be treated as Lennard-Jones particles, the bulk fluid will freeze at a temperature that is proportional to the parameter $\varepsilon_{ff}$. Similarly, we can expect that the freezing temperature for the confined phase will be proportional to $\varepsilon_{\text{eff}}$, which is an effective energy parameter that accounts for both the fluid-fluid and fluid-wall interactions in some average way. For strongly attractive walls, an increase in the freezing temperature with respect to the bulk is expected as $\varepsilon_{\text{eff}}$ is larger than $\varepsilon_{ff}$. In contrast, a decrease in the freezing temperature is expected for weakly attractive pores as $\varepsilon_{\text{eff}}$ is smaller than $\varepsilon_{ff}$. When $\varepsilon_{\text{eff}} \sim \varepsilon_{ff}$, the in-pore freezing temperature should be similar to the bulk. These predictions are supported by previous molecular simulations and experiments on freezing and melting of simple fluids confined in various nanoporous materials (carbon pores, silica pores, mica plates in surface force apparatus, etc.).[12,13,16–23] Since carbon and mica surfaces are strongly attractive, we expect that a rise in freezing temperature is likely for many adsorbates that do not have strongly attractive (e.g., H-bonding) fluid-fluid interactions. Such systems exhibit large $\alpha$ values, i.e., the ratio of the wall-fluid to the fluid-fluid interactions is larger than 1. On the other hand, we would not expect such an increase in $T_f$ for water in these materials since $\alpha$ is smaller than 1.[12,13] Recent surface force apparatus (SFA) experiments have confirmed this prediction by showing that water[24,25] and some alcohols (octanol and undecanol)[26] remain fluidlike even for confined film thicknesses below 1 nm.

In contrast to the large amount of work devoted to understanding freezing of pure fluids confined in nanopores, the case of binary mixtures has received considerably less attention.[27–32] In previous works,[30–32] we studied the confinement effect on freezing/melting of mixtures confined in graphite slit nanopores by means of Monte Carlo molecular simulations and experiments. We found that the phase diagram for the confined mixture was of the same type as that for the bulk, but the solid/liquid coexistence lines were located at higher temperatures. This result was expected since the $\alpha$ parameter for the systems investigated is larger than 1. In this paper, we report experiments and molecular simulations for binary mixtures confined in silica nanopores. The experimental measurements consist of differential scanning calorimetry and dielectric relaxation spectroscopy for $CCl_4/C_6H_5Br$ confined in Vycor having pores with a diameter of $D=4.2$ nm. The latter pore size corresponds to a reduced pore size $D^*=D/\sigma \sim 8.2$ [where $\sigma$ is the size of the adsorbate, $\sigma_{CCl_4}=0.514$ nm and $\sigma_{C_6H_5Br} \sim 0.5$ nm (Ref. 13)]. The molecular simulations were performed for Lennard-Jones Ar/Kr mixtures confined within a cylindrical nanopore having a pore diameter of $D=3.2$ nm, which corresponds to a reduced size of $D^* \sim 9.4\sigma_{Ar}$, in the same range as that considered in the experiments. Following previous works on the freezing of pure substances, we study the structure of the confined phase using local bond order parameters and positional pair correlation functions. This paper is organized as follows. In Sec. II, we present details of the experimental and molecular simulation techniques. In Sec. III, we first discuss our experimental results for melting of $CCl_4/C_6H_5Br$ mixtures confined in Vycor. We then present data obtained from molecular simulations of freezing of Ar/Kr confined in a cylindrical silica nanopore. In Sec. IV, we summarize our results and suggest future works.

## II. METHODS

### A. Experiment

Vycor having a mean pore diameter of 4.2 nm was used in this work to study the melting upon confinement of $C_6H_5Br/CCl_4$ mixtures. Pores in this material, which are approximately of a cylindrical geometry, are expected to accommodate about approximately eight layers of $CCl_4$ or $C_6H_5Br$ since the reduced pore width is $D^* \sim 8.2$ (using either the size of $CCl_4$ or $C_6H_5Br$). $CCl_4$ and $C_6H_5Br$ were distilled twice prior to their use in experiments. Samples were outgassed during 5 days at a temperature of 150 °C and under a vacuum of $10^{-4}$ Torr, prior to introduction of the mixture. Dielectric relaxation spectroscopy (DRS) of the confined mixture was performed using a parallel plate capacitor of empty capacitance $C_0=69.1$ pF. The capacitance $C$ and the tangent loss $\tan(\delta)$ (where $\delta$ is the angle by which current leads the voltage) of the filled sample were measured at different temperatures using a Solartron 1260 impedance/gain phase analyzer in the frequency range of 10 Hz–10 MHz. The real and imaginary parts of the complex dielectric permittivity $\varepsilon^*=\varepsilon' \iota \varepsilon''$ are related to the capacitance and tangent loss of the system, $\varepsilon'=C/C_0$ and $\varepsilon''=\tan(\delta)/\varepsilon'$.[33,34] Melting of a solid phase can be monitored in the DRS experiment by a large increase of the permittivity. The sample was introduced between the capacitor plates as a suspension of Vycor filled with the mixture in the bulk mixture. Therefore, the measurements yield an effective permittivity that has contributions from the bulk and the confined mixtures. During the experiments, the temperature of the sample was controlled with an accuracy of 0.1 K using a cryostat MK-70. The mass of the samples used in the dielectric experiments was about 250–300 mg.

A PerkinElmer DSC7 was used to determine the melting temperatures by measuring the heat release in the melting of confined $C_6H_5Br/CCl_4$ mixtures. The temperature scale of the differential scanning calorimeter (DSC) was calibrated to the melting temperatures of pure $CCl_4$ and $C_6H_5Br$, respectively. Temperature scanning rates of 2–5 K/min were used in the experiments. The weight of the sample, which consists of a suspension of mixture-filled Vycor in the pure mixture, was about 0.5–0.7 mg. The melting temperatures were determined from the positions of the peaks of the heat flow signal. The melting temperatures were reproducible to within 0.5 K.

### B. Molecular simulation

The atomistic silica nanopore used in this work was generated according to the method proposed by Pellenq and Levitz to prepare numerical Vycor samples.[35] It has been shown that this technique can be used to prepare pores of various morphologies and/or topologies, such as cylindrical, hexagonal, ellipsoidal, and constricted pores.[36–39] The cylindrical nanopore used in this work was carved out of an atomistic block of cristobalite (crystalline silica). In order to mimic the pore surface in a realistic way, we removed in a second step the Si atoms that are in an incomplete tetrahedral environment. We then removed all oxygen atoms that are nonbonded. This procedure ensures that the remaining silicon atoms have no dangling bonds and the remaining oxygen atoms have at least one saturated bond with a Si atom. Then, the electroneutrality of the simulation box was ensured by saturating all oxygen dangling bonds with hydrogen atoms. The latter is placed in the pore void, perpendicular to the pore surface, at a distance of 1 Å from the closest unsaturated oxygen atom. Then, we displace slightly and randomly all the O, Si, and H atoms in order to mimic an amorphous silica surface (the maximum displacement in each direction $x$, $y$, and $z$ is 0.7 Å). We studied the freezing of Ar/Kr mixtures confined in a silica nanopore with a diameter of $D=3.2$ nm $(9.4\sigma_{Ar})$. Periodic boundary conditions were applied in the $z$ direction parallel to the pore axis. The pore diameter $D$ corresponds to the diameter used to initially carve out the nanopore: Si and O atoms beyond this value are kept. Given that hydrogens are then added at the pore surface to saturate the O dangling bonds, an estimate of the pore diameter $\tilde{D}$ accessible to the confined mixture is given by the initial pore diameter $D$ diminished by two times the size of the OH bond (0.1 nm) and the excluded radius of the interaction between Ar $(\sigma_{Ar/H}\sim 0.30$ nm) or Kr $(\sigma_{Kr/H}\sim 0.32$ nm) and the hydrogen atoms, i.e., $\tilde{D}=D-2d_{OH}-\sigma$. Adopting this definition, we find $\tilde{D}=2.7$ nm for argon and 2.6 nm for krypton.

The behavior of an Ar/Kr mixture confined in the silica cylindrical pore was determined using the grand canonical Monte Carlo (GCMC) technique. This stochastic method simulates a system having a constant volume $V$ (the pore with the adsorbed phase), in equilibrium with an infinite fictitious reservoir of particles that imposes its chemical potential for each species, $\mu_A$ and $\mu_B$, and its temperature, $T$.[40–42] The chemical potentials $\mu_{Ar}$ and $\mu_{Kr}$ were calculated so that the confined mixture is, for all pressures and temperatures, in equilibrium with a bulk ideal gas mixture with $x_{Ar}=0.999$ (as will be discussed below, due to the relative affinities of Ar and Kr for silica, the composition of the confined mixture will be closer to that of an equimolar mixture). Particle displacement, insertion, and deletion were attempted randomly in the course of the simulations. The sampling of the phase space was improved by adding a fourth move that consists of exchanging the identity of an existing particle. In order to circumvent the difficulty of particle deletion and insertion in dense phases such as liquids and solids, we combined the GCMC simulations with the parallel tempering technique.[43,44] This method consists of considering several replicas of the system at different temperatures and chemical potentials. In addition to conventional Monte Carlo moves that are performed for each replica, trial swap moves between configurations in different replicas are attempted. The parallel tempering technique prevents the system from being "trapped" in local metastable states.[30–32,45–48] Full details of the GCMC and parallel tempering techniques used in this work have been described elsewhere.[30,32] The number of particles in our simulations varies from 1000 to 6000, depending on the mole fraction of the confined mixture. The number of replicas used in this work is 16 and the temperature difference between two successive replicas is $\Delta T=2$ or 3 K. We started with well equilibrated liquid configurations of the confined mixture and performed, at least, $10^5$ Monte Carlo steps per particle to equilibrate the system using the parallel tempering technique. After equilibration of the system, density profiles, bond order parameters, and pair correlation functions were averaged in the course of a second simulation run.

The Ar/Ar and Kr/Kr interactions were calculated using Lennard-Jones potentials with the following parameters: $\sigma_{Ar/Ar}=0.3405$ nm, $\varepsilon_{Ar/Ar}/k=120.0$ K and $\sigma_{Kr/Kr}=0.369$ nm, $\varepsilon_{Kr/Kr}/k=170.0$ K. The cross-species Ar/Kr parameters were calculated using the Lorentz–Berthelot combining rules.[49] The Lennard-Jones potentials were truncated at a distance of half the size of the simulation box. Interactions between the argon or krypton atoms and the atoms of the silica substrate were calculated using the PN-TraZ potential as reported for rare gas adsorption in zeolite[50] or in porous silica glass.[35] The intermolecular energy is written as the sum of the dispersion interaction with a repulsive short-range contribution and an induction term due to the interaction of the adsorbed atom with the local field created by the partial charges of the atoms in the substrate. Values of the interaction parameters as well as details of the intermolecular potential functions can be found in the previous work by Pellenq and Levitz.[35] We calculated the adsorbate/substrate interaction using an energy grid;[51] the potential energy is calculated at each corner of each elementary cube (about 1 $Å^3$). An accurate estimate of the energy is then obtained by a linear interpolation of the grid values. Such a procedure enables simulation of adsorption in mesoporous media of complex morphology and/or topology without a direct summation over matrix species in the course of GCMC runs.

Strong layering was observed due to the interaction with the attractive pore walls. Following the previous works on freezing of pure fluids in nanopores,[47,48,13,52,53] the structure of the confined mixture was investigated by calculating for each layer $i$ the density and the positional pair correlation functions, $g_i(r)$.

## III. RESULTS AND DISCUSSION

### A. Experiment

Melting of $C_6H_5Br/CCl_4$ for bulk mixtures and confined in Vycor was determined by monitoring changes in the dielectric permittivity $\varepsilon$. Freezing of dipolar liquids such as bromobenzene is accompanied by a rapid decrease in $\varepsilon'$ (the real part of the dielectric permittivity). Below the freezing

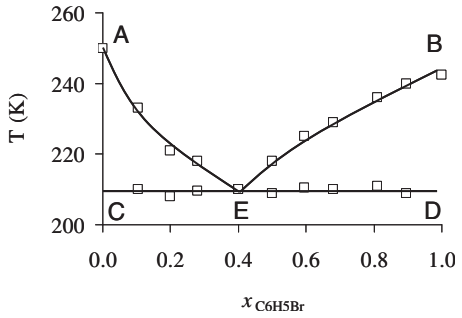


FIG. 1. Solid-liquid phase diagram $(T,x_2)$ at a constant pressure $P=1$ atm for bulk $C_6H_5Br/CCl_4$ mixtures. ($x_2$ is the bromobenzene mole fraction). The lines between the symbols are provided as a guide for the eye.

point, the rotational phase ceases to exist and $\varepsilon'$ is almost equal to $n^2$ ($n$ is the refractive index) as it is only related to deformation polarization. On the other hand, the maximum value $\varepsilon'_m$ of the permittivity is obtained for the liquid phase. As a result, $\varepsilon'_m$ and $\varepsilon'_s$ (the real part of the permittivity in the solid phase) can be determined by measuring the functions $\varepsilon'(T)$ or $C(T)$ ($C$ is the electric capacity of the system) in the vicinity of the melting point of a dipolar liquid. In turn, the determination of the temperature at which changes are observed in $\varepsilon(T)$ or $C(T)$ allows us to estimate transition temperatures of the system. Figure 1 shows the phase diagram of the bulk $C_6H_5Br/CCl_4$ mixture at $P=1$ atm. Such a phase diagram is a characteristic of a simple eutectic mixture. The lines AEB were obtained from the temperature $T_1$ at which the entire system is in the liquid state. The lines AE and BE correspond to the temperatures at which the liquid mixture is in equilibrium with a solid phase. The line CD was obtained from the temperature $T_2$ at which the system starts melting. The eutectic E indicates the point where the solid constituent rich in $C_6H_5Br$ and that rich in $CCl_4$ are in equilibrium with the liquid phase having a composition $x_2^E \sim 0.41$. In the case of $C_6H_5Br/CCl_4$ mixtures, the melting points of the two components are rather close (bromobenzene at 242.3 K and carbon tetrachloride at 252.4 K) so that the eutectic concentration $x_2^E$ is close to 0.5, which suggests that the properties of the system are close to those of the model of ideal miscibility.

Figure 2 shows the capacity curve $C(T)$ as a function of temperature for $C_6H_5Br/CCl_4$ mixtures confined in Vycor. Data for confined mixtures in equilibrium with a bulk mixture with $x_{C_6H_5Br}{}^0 \sim 0.80$ and $x_{C_6H_5Br}{}^0 \sim 0.60$ are shown. For a given composition, two changes are observed in the slope of the $C(T)$ curve; the latter is a characteristic of bulk mixtures as it corresponds to the solidus $T_1$ and liquidus $T_2$ of the system. Besides these two phase transitions for the bulk mixture, $C(T)$ is a monotonous increasing function of temperature that does not exhibit any sharp change. This result suggests that the confined mixture does not undergo any first order phase transition such as crystallization. The same conclusion was reached for all concentrations.

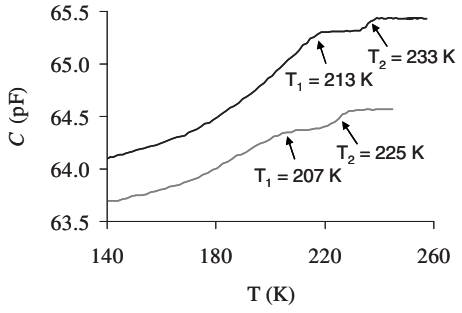


FIG. 2. Capacity curve $C(T)$ as a function of temperature for $C_6H_5Br/CCl_4$ mixture confined in Vycor. The black and gray lines are for confined mixtures in equilibrium with a bulk mixture with $x_{C_6H_5Br}{}^0 \sim 0.80$ and $x_{C_6H_5Br}{}^0 \sim 0.60$, respectively.

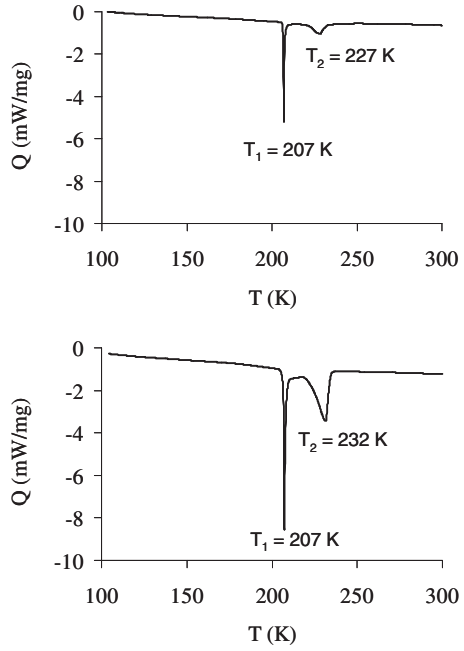


FIG. 3. Differential scanning calorimetry scan upon melting of a $C_6H_5Br/CCl_4$ mixture confined in Vycor. (Top) The confined mixture is in equilibrium with a bulk mixture with $x_{C_6H_5Br}{}^0 \sim 0.60$. (Bottom) The confined mixture is in equilibrium with a bulk mixture with $x_{C_6H_5Br}{}^0 \sim 0.55$.

In order to confirm the absence of crystallization suggested by DRS, we also performed DSC for $C_6H_5Br/CCl_4$ mixtures confined in Vycor having pores with an average diameter of $D=4.2$ nm. DSC scans upon heating of $C_6H_5Br/CCl_4$ mixtures in Vycor are shown in Fig. 3. The confined mixture is in equilibrium with bulk mixtures having a composition of $x_{C_6H_5Br}{}^0 \sim 0.60$ or $x_{C_6H_5Br}{}^0 \sim 0.55$. For both compositions, the DSC scan exhibits two endothermic peaks located at temperatures $T_1$ and $T_2$. The latter temperatures reveal melting of the bulk $C_6H_5Br/CCl_4$ mixture as they correspond for a given concentration to the solidus and liquidus transitions, respectively. $T_1$ and $T_2$, which correspond to the solidus and liquidus transition temperatures, are related to crystallization of $CCl_4$ and bromobenzene, respectively. Upon melting, the DSC peak observed at $T_2$ is sharp as it arises from the large contribution of the permanent dipole of bromobenzene to the orientational polarization of the liquid state. On the other hand, the DSC peak is less marked at $T_1$ as, for nonpolar liquids such as $CCl_4$, it only corresponds to the energy change when the density of the system varies with temperature. Besides the two peaks at $T_1$ and $T_2$, no additional peak is observed in the DSC scans, which suggests that crystallization of the mixtures confined in Vycor is suppressed.

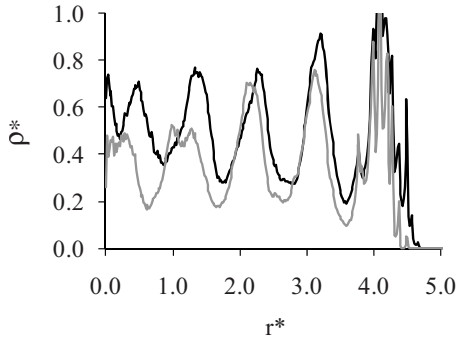


FIG. 4. Density profiles for an Ar/Kr mixture confined in a silica cylindrical nanopore with $D=9.4\sigma_{Ar}$ at $T^*=0.46$. The black and gray lines are for argon and krypton, respectively. The density for both Ar and Kr are plotted on the same scale. For all temperatures, the confined mixture is in equilibrium with a bulk mixture with $x_{Ar}{}^0 \sim 0.999$. Distances and densities are in reduced units with respect to $\sigma_{Ar}$ and $\varepsilon_{Ar}$.

### B. Molecular simulation

We now discuss the molecular simulation results obtained for an Ar/Kr mixture confined in a cylindrical nanopore with reduced diameter of $D=9.4\sigma_{Ar}$ (3.2 nm). Such a pore diameter is close to the average pore size for Vycor samples, $D=4.2$ nm. The radial density profiles $\rho(r^*)$ of the confined Ar/Kr mixture are shown in Figs. 4 and 5 for $T^*=0.46$ and $T^*=0.83$, respectively. $r^*$ is the distance from the center of the cylindrical pore in reduced units with respect to the Lennard-Jones parameter $\sigma_{Ar}$. The density profiles exhibit five oscillations corresponding to different layers of the confined mixture. In what follows, the three outer layers will be referred to as contact, second, and third layers, respectively, and the fourth and innermost layers will be considered together as we expect them to behave similarly upon freezing. Integrating the density profiles shown in Figs. 4 and 5 show that the confined mixture has a larger Kr mole fraction than the bulk mixture, $x_{Kr}=0.001$, for all temperatures. This result is due to the fact that Kr has larger average interaction energy with silica (17.5 kJ/mol) than Ar (13 kJ/mol). This result is in agreement with the previous simulation and theoretical works, showing that the molar composition of the component having the strongest interaction with the pore wall is increased compared to the bulk.

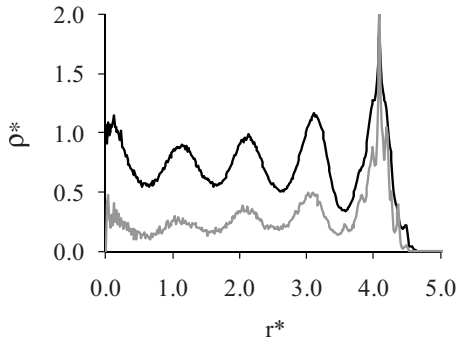


FIG. 5. Density profiles for an Ar/Kr mixture confined in a silica cylindrical nanopore with $D=9.4\sigma_{Ar}$ at $T^*=0.83$. The black and gray lines are for argon and krypton, respectively. Because the Kr concentration is very low at this temperature (see Fig. 7), the density profile for krypton has been multiplied by 10 for the sake of clarity. For all temperatures, the confined mixture is in equilibrium with a bulk mixture with $x_{Ar}{}^0 \sim 0.999$. Distances and densities are in reduced units with respect to $\sigma_{Ar}$ and $\varepsilon_{Ar}$.

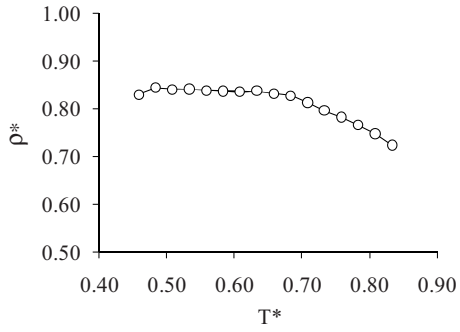


FIG. 6. Average density for an Ar/Kr mixture confined in a silica cylindrical nanopore with $D=9.4\sigma_{Ar}$ as a function of temperature. For all temperatures, the confined mixture is in equilibrium with a bulk mixture with $x_{Ar}{}^0 \sim 0.999$. Temperatures and densities are in reduced units with respect to $\sigma_{Ar}$ and $\varepsilon_{Ar}$.

Figure 6 shows the average particle density for the Ar/Kr mixture confined in the silica cylindrical nanopore with $D=9.4\sigma_{Ar}$ as a function of temperature. As mentioned above, the pore diameter $D$ corresponds to the diameter used to initially carve out the nanopore. Taking into account the excluded radius of the interaction between Ar or Kr ($\sigma_{Kr/H} \sim 0.32$ nm) and the pore surface, the pore diameter $\tilde{D}$ accessible to the confined mixture is 2.7 nm for argon and 2.6 nm for krypton. We also show in Fig. 7 the Ar mole fraction $x_{Ar}$ of the confined mixture as a function of temperature. The particle density is nearly insensitive to the temperature in the range of $T^*=0.4-0.65$ and then decreases with increasing temperature in the range of $T^*=0.65-0.85$. Such a temperature dependence can be explained on the basis of the change in the composition of the confined mixture as $T^*$ increases. For $T^*=0.65-0.85$, $x_{Ar}$ varies slowly with temperature (nearly constant) so that $\rho^*$ decreases with increasing $T^*$ as expected for liquids. In contrast, for $T^*=0.4-0.65$, $x_{Ar}$ increases more rapidly with $T^*$ so that $\rho^*$ is nearly constant as the density decrease with increasing $T^*$ is counterbalanced by the particle density increase when changing the molar composition of the mixture (due to the size difference between Ar and Kr, Kr atoms in the pore volume are replaced by a larger number of Ar atoms). We note that such a temperature dependence of $x_{Ar}$ and $\rho^*$ is not driven by confinement or surface effects as the same behavior is observed for the bulk mixture (see the change in the curvature of the liquid coex-

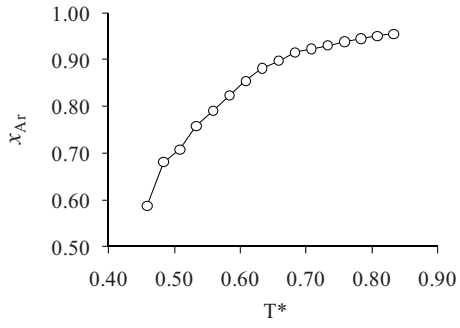


FIG. 7. Ar mole fraction for an Ar/Kr mixture confined in a silica cylindrical nanopore with $D=9.4\sigma_{Ar}$ as a function of temperature. For all temperatures, the confined mixture is in equilibrium with a bulk mixture with $x_{Ar}{}^0 \sim 0.999$. Temperatures are in reduced units with respect to $\varepsilon_{Ar}$.

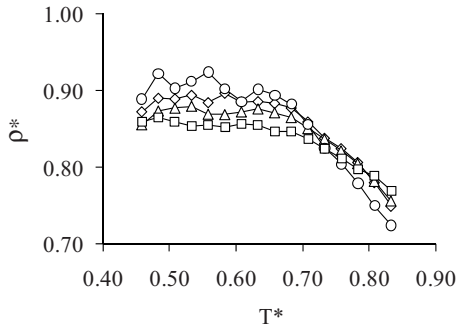


FIG. 8. Average density for each layer of an Ar/Kr mixture confined in a silica cylindrical nanopore with $D=9.4\sigma_{Ar}$ as a function of temperature: (circles) inner part of the pore corresponding to the fourth and fifth layers, (diamonds) third layer, (triangles) second layer, and (squares) contact layer. For all temperatures, the confined mixture is in equilibrium with a bulk mixture with $x_{Ar}{}^{0}\sim 0.999$. Temperatures and densities are in reduced units with respect to $\sigma_{Ar}$ and $\varepsilon_{Ar}$.

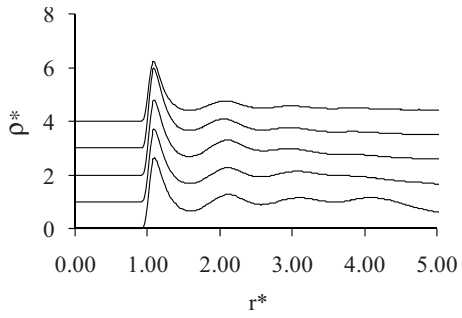


FIG. 9. 2D pair correlation functions $g(r)$ for the layers of an Ar/Kr mixture confined in a silica cylindrical nanopore with $D=9.4\sigma_{Ar}$ at $T^{*}=0.83$: (from top to bottom) contact, second, third, fourth, and fifth layers. For all temperatures, the confined mixture is in equilibrium with a bulk mixture with $x_{Ar}{}^{0}\sim 0.999$. Distances and densities are in reduced units with respect to $\sigma_{Ar}$ and $\varepsilon_{Ar}$. For the sake of clarity, the $g(r)$ functions for the second, third, fourth, and fifth layers have been shifted by +1, +2, +3, and +4, respectively.

istence line of the bulk Ar/Kr phase diagram in Fig. 1 of Ref. 30). In particular, the absence of sharp changes in the mixture composition or overall density suggests that no crystallization occurs upon cooling of the confined system. This result contrasts with our previous works[30–32] for mixtures in regular slit nanopores in which crystallization was found for the different layers of the confined system. On the other hand, the absence of crystallization for mixtures confined in the cylindrical nanopore with $D=9.4\sigma_{Ar}$ is consistent with the previous work by Sliwinska-Bartkowiak *et al.*[34] These authors showed that even partial crystallization does not occur for cylindrical nanopores smaller than $D=15\sigma$. Such a "frustrating" or "hindering" effect of the cylindrical geometry compared to the slit geometry has been discussed in the previous simulation works by Maddox and Gubbins,[23] Hung *et al.*,[53] and Kuchta *et al.*[54]

In order to investigate in deeper detail the behavior of the confined system upon cooling, we show in Fig. 8 the average density for each layer of the Ar/Kr mixture in the silica cylindrical nanopore with $D=9.4\sigma_{Ar}$ as a function of temperature. Very similar trends are observed for the different layers and the innermost region of the confined mixture as the temperature decreases. This result indicates that the different regions of the confined mixture behave similarly upon cooling. In particular, the absence of a sharp change in the density of the layers when the temperature decreases confirms that no crystallization of the confined layers occur for such a small cylindrical pore ($D=9.4\sigma_{Ar}$). In-plane two-dimensional (2D) positional $g(r)$ pair correlation functions for the different confined layers at two temperatures are presented in Figs. 9 and 10, respectively. Correlations within each layer were determined up to a distance of half the size of the simulation box. The positional pair-correlation function $g_i(r)$ is given for a confined layer $i$ by the radial distribution function measured only for atoms belonging to the layer. At $T^{*}=0.83$, the confined layers exhibit a liquidlike behavior as revealed by the $g(r)$ function, which is a characteristic of a phase having short-range positional order. At $T^{*}=0.46$, the confined layers also exhibit short-range order, although some features of a crystal phase are reminiscent of the bulk crystallization. For instance, the second peak corresponding to the second nearest neighbor is asymmetrical. We note that this feature is more pronounced for the mixture in the second, third, and innermost layers than for the contact layer, which indicates that the presence of the silica surface induces some disorder in the structure of the atoms located in the contact layer. Similar results have been observed in the case of benzene in the vicinity of a silica surface or nanopore;[55,56] benzene tends to disorganize its structure to favor its interaction with the substrate. Despite the vanishing/reminiscent short-range crystalline features observed for the confined layers, our results suggest that no crystallization occurs for the mixture confined in the cylindrical nanopore with $D=9.4\sigma_{Ar}$. This result is also in agreement with the previous work by Sliwinska-Bartkowiak *et al.*,[34] showing that no crystallization occurs for the contact layer of systems confined in cylindrical nanopores with diameters smaller than $15\sigma$. The absence of crystallization is confirmed by direct visualization in Fig. 11 of typical molecular configurations of the Ar/Kr confined mixture. We note that due to the use of an initial crystalline block to prepare the porous material, the "cylindrical" pore corresponds to a pore with an octagonal section rather than with a regular circular section. This octagonal section arises from the cutting procedure as it

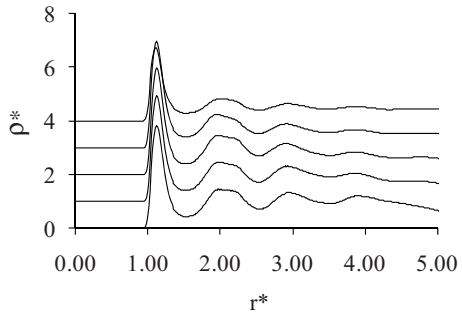


FIG. 10. 2D pair correlation functions $g(r)$ for the layers of an Ar/Kr mixture confined in a silica cylindrical nanopore with $D=9.4\sigma_{Ar}$ at $T^{*}=0.46$: (from top to bottom) contact, second, third, fourth, and fifth layers. For all temperatures, the confined mixture is in equilibrium with a bulk mixture with $x_{Ar}{}^{0}\sim 0.999$. Distances and densities are in reduced units with respect to $\sigma_{Ar}$ and $\varepsilon_{Ar}$. For the sake of clarity, the $g(r)$ functions for the second, third, fourth, and fifth layers have been shifted by +1, +2, +3, and +4, respectively.

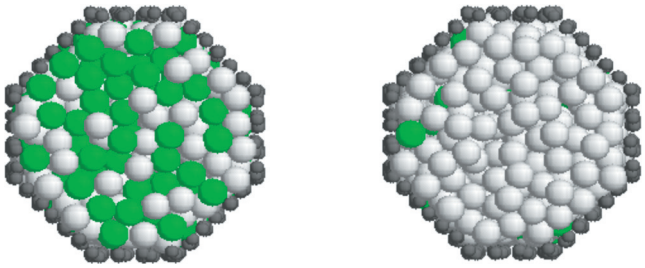

FIG. 11. Typical molecular configuration for an Ar/Kr mixture confined in a silica cylindrical nanopore with $D=9.4\sigma_{Ar}$ at $T^*=0.46$ (left) and $T^*=0.83$ (right). The white and green spheres are the argon and krypton atoms, respectively. The gray spheres are the hydrogen atoms that delimitate the pore surface.

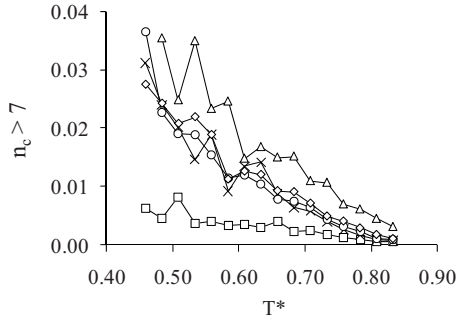


FIG. 12. Fraction of crystal-like atoms as a function of the temperature $T^*$ for the layers of an Ar/Kr mixture confined in a silica cylindrical nanopore with $D=9.4\sigma_{Ar}$: (squares) contact layer, (triangles) second layer, (diamonds) third layer, (circles) fourth layer, and (crosses) fifth layer.

corresponds to the mathematical intersection between the regular circular interface and the crystalline planes of cristobalite.

We also confirmed the absence of crystallization by calculating the *local* order parameter proposed by ten Wolde *et al.*[57] to distinguish particles that are liquidlike or crystal-like. For each atom $i$ of the confined phase, we calculated the 13 normalized parameters $\tilde{q}_{6m}(i)$ that are defined as

$$\tilde{q}_{6m}(i) = \frac{A}{N_b(i)} \sum_{j=1}^{N_b(i)} Y_{6m}(\mathbf{r}_{ij}) \quad \text{with} \quad m \in [-6,6], \tag{1}$$

where $\mathbf{r}_{ij}$ are the vectors joining atom $i$ and each of its $N_b(i)$ neighbors $j$. $A=[\Sigma_{m=-6}^{6}|\overline{q_{6m}}(i)|^2]^{-1/2}$ is the normalization constant. In contrast to global order parameters that are usually used to study freezing of bulk compounds, $\tilde{q}_{6m}(i)$ is a local quantity that depends only on atom $i$ and its neighbors $j$. For each pair of nearest neighbors, we define the following scalar product:[57]

$$\mathbf{q}_6(i) \cdot \mathbf{q}_6(j) = \sum_{m=-6}^{6} \tilde{q}_{6m}(i)\tilde{q}_{6m}(j)^*. \tag{2}$$

Atoms $i$ and $j$ can be considered "connected" in a coherent manner if the product $\mathbf{q}_6(i)\cdot\mathbf{q}_6(j)$ is larger than or equal to 0.5. ten Wolde *et al.* showed that an atom $i$ in a three-dimensional environment is crystal-like if it is connected in a coherent manner to at least seven of its nearest neighbors; this definition ensures that liquid and bcc or fcc crystal structures are unambiguously distinguished.[57] It has been shown recently that this local order parameter can be used to describe freezing of fluids confined in disordered porous structures.[58,59] Figure 12 shows the fraction of crystal-like atoms as a function of the temperature $T^*$ for the layers of the Ar/Kr mixture confined in a silica cylindrical nanopore with $D=9.4\sigma_{Ar}$. For all layers, the percentage of crystal-like atoms is always less than 5%, which confirms the absence of crystallization for the confined mixture. Interestingly, the fraction of crystal-like atoms for the contact layer is, for all temperatures, about half the value for the other layers. This result is consistent with the fact that even at low temperature, the reminiscent features of a crystal phase for this layer are less marked than for the other layers (Fig. 10). As mentioned above, this is due to the presence of the silica surface that induces some disorder in the structure of the atoms located in the contact layer. In particular, although the contact layer has the larger density, atoms in this layer are less ordered than in the second layer. In fact, despite its large density arising from the strong interaction with the silica wall, the contact layer tends to be disordered due to the surface roughness of the substrate. In contrast, despite its smaller density, the second layer is more ordered as it also benefits from the strong interaction with the silica wall without being affected by the surface roughness of the silica wall.

## IV. CONCLUSION AND FUTURE WORK

Our findings can be summarized as follows. Simulations and experiments, which are for pore diameters in the range of $D\sim 7\sigma-10\sigma$ ($\sigma$=diameter of adsorbate molecule), are in qualitative agreement. Both series of results suggest that crystallization of mixtures is suppressed upon confinement in pores of a reduced size lower than $10\sigma$. No sharp change in the composition, density, or dielectric properties of the different confined mixtures occurs upon cooling, which suggests that the confined system does not crystallize. Molecular simulation further supports this conclusion as, for all layers of confined mixtures, the percentage of crystal-like atoms in the molecular simulation is always less than 5% (whatever the temperature). GCMC simulations also show that the composition of the mixture is shifted, upon confinement, toward the component having the largest wall/fluid interaction. It was not possible to verify such a trend in the case of the experiments because of the lack of knowledge of the molar composition within the pore (only the global mole fraction bulk/confined mixture is known).

The above results are consistent with the previous works reported in literature on the freezing of pure fluids confined in cylindrical nanopores. For instance, Maddox and Gubbins[23] found that crystallization of Lennard-Jones fluids confined in smooth cylindrical nanopores is frustrated due to strong geometrical constraints. Later, Sliwinska-Bartkowiak and co-workers[34] showed that a fluid confined in a cylindrical nanopore freezes into a single crystalline structure for average pore diameters larger than $20\sigma$. In contrast, fluids[34] or mixtures[60] in pores with a diameter between $15\sigma$ and $20\sigma$ crystallize into a frustrated crystal structure with the rest forming an amorphous region. Finally, for pore sizes smaller than $15\sigma$, even partial crystallization does not occur. A dif-

ference between our findings and the results reported in these previous works concerns solidification of the confined layer. In the present work, no crystallization of the contact layer is observed due to the use of an atomistically rough substrate, which imposes some disorder in the local organization of the atoms located in the contact layer. Even for large pores with $D > 20\sigma$ (results not shown), freezing of the contact layer is not observed as its structure remains liquidlike. In contrast, the authors in Refs. 23 and 34 used silica walls described as an assembly of smooth Lennard-Jones spheres which favor the layering and ordering of the adsorbed phase. The difference in the pressures used in these different works may also affect the crystallinity and freezing behavior of the confined system. This idea is supported by recent works,[61–66] in which it has been shown that in-pore freezing strongly depends on pressure due to the capillary effect (i.e., the in-pore pressure varies strongly with the bulk external pressure).

In future work, we plan to determine the behavior of different types of mixtures (such as azeotropic or eutectic mixtures) confined in silica nanopores. We will also estimate the effect of surface disorder by considering pores with morphological defects such as a constriction or a distorted section. In this regard, realistic models of such cylindrical silica nanopores, which are available in literature, are of particular interest.[39,67] Such models permit an estimate of the effect of surface chemistry to be made by considering different silica substrates (fully or partially hydroxylated surfaces, presence of siloxane groups, etc.).[38]


[1] H. Masuda and K. Fukuda, Science **268**, 1466 (1995).
[2] P. M. Ajayan, O. Stephan, Ph. Redlich, and C. Colliex, Nature (London) **375**, 564 (1995).
[3] P. J. F. Harris, *Carbon Nanotubes and Related Structures. New Materials for the Twenty-First Century* (Cambridge University Press, Cambridge, 1999).
[4] J. Sloan, M. C. Novotny, S. R. Bailey, G. Brown, C. Xu, V. C. Williams, S. Fredrichs, E. Flahaut, R. L. Callender, A. P. E. York, K. S. Coleman, M. L. H. Green, R. E. Dunin-Borkowski, and J. L. Hutchison, Chem. Phys. Lett. **329**, 61 (2000).
[5] A. A. Zhakidov, R. H. Baughman, Z. Iqbal, and C. X. Cui, Science **282**, 897 (1998).
[6] Z. B. Zhang, D. Gekhtman, M. S. Dresselhaus, and J. Y. Ying, Chem. Mater. **11**, 1659 (1999).
[7] M. Alcoutlabi and G. B. McKenna, J. Phys.: Condens. Matter **17**, R461 (2005).
[8] C. Alba-Simionesco, B. Coasne, G. Dosseh, G. Dudziak, K. E. Gubbins, R. Radhakrishnan, and M. Sliwinska-Bartkowiak, J. Phys.: Condens. Matter **18**, R15 (2006).
[9] B. Coasne, A. Mezy, R. J. M. Pellenq, D. Ravot, and J. C. Tedenac, J. Am. Chem. Soc. **131**, 2185 (2009).
[10] C. Eyraud, J. F. Quinson, and M. Brun, in *Characterization of Porous Solids*, edited by K. Unger, J. Rouquerol, K. S. W. Sing, and H. Kral (Elsevier, Amsterdam, 1988), p. 307.
[11] L. D. Gelb, K. E. Gubbins, R. Radhakrishnan, and M. Sliwinska-Bartkowiak, Rep. Prog. Phys. **62**, 1573 (1999).
[12] R. Radhakrishnan, K. E. Gubbins, and M. Sliwinska-Bartkowiak, J. Chem. Phys. **112**, 11048 (2000).
[13] R. Radhakrishnan, K. E. Gubbins, and M. Sliwinska-Bartkowiak, J. Chem. Phys. **116**, 1147 (2002).
[14] J. Warnock, D. D. Awschalom, and M. W. Shafer, Phys. Rev. Lett. **57**, 1753 (1986).
[15] R. Evans and U. Marini Bettolo Marconi, J. Chem. Phys. **86**, 7138 (1987).
[16] M. Sliwinska-Bartkowiak, J. Gras, R. Sikorski, R. Radhakrishnan, L. D. Gelb, and K. E. Gubbins, Langmuir **15**, 6060 (1999).
[17] R. Radhakrishnan, K. E. Gubbins, A. Watanabe, and K. Kaneko, J. Chem. Phys. **111**, 9058 (1999).
[18] J. Klein and E. Kumacheva, Science **269**, 816 (1995).
[19] E. Kumacheva and J. Klein, J. Chem. Phys. **108**, 7010 (1998).
[20] A. Watanabe and K. Kaneko, Chem. Phys. Lett. **305**, 71 (1999).
[21] K. Kaneko, A. Watanabe, T. Iiyama, R. Radhakrishnan, and K. E. Gubbins, J. Phys. Chem. B **103**, 7061 (1999).
[22] M. Miyahara and K. E. Gubbins, J. Chem. Phys. **106**, 2865 (1997).
[23] M. Maddox and K. E. Gubbins, J. Chem. Phys. **107**, 9659 (1997).
[24] U. Raviv, P. Laurat, and J. Klein, Nature (London) **413**, 51 (2001).
[25] U. Raviv, S. Giasson, J. Frey, and J. Klein, J. Phys.: Condens. Matter **14**, 9275 (2002).
[26] F. Mugele, B. Persson, S. Zilberman, A. Nitzan, and M. Salmeron, Tribol. Lett. **12**, 123 (2002).
[27] R. R. Meyer, J. Sloan, R. E. Dunin-Borkowski, A. I. Kirkland, M. C. Novotny, S. R. Bailey, J. L. Hutchinson, and M. L. H. Greene, Science **289**, 1324 (2000).
[28] M. Wilson, J. Chem. Phys. **116**, 3027 (2002).
[29] S. T. Cui, C. McCabe, P. T. Cummings, and H. D. Cochran, J. Chem. Phys. **118**, 8941 (2003).
[30] B. Coasne, J. Czwartos, K. E. Gubbins, F. R. Hung, and M. Sliwinska-Bartkowiak, Mol. Phys. **102**, 2149 (2004).
[31] B. Coasne, J. Czwartos, K. E. Gubbins, F. R. Hung, and M. Sliwinska-Bartkowiak, Adsorption **11**, 301 (2005).
[32] J. Czwartos, B. Coasne, K. E. Gubbins, F. R. Hung, and M. Sliwinska-Bartkowiak, Mol. Phys. **103**, 3103 (2005).
[33] A. Chelkowski, *Dielectric Physics* (Elsevier, New York, 1980).
[34] M. Sliwinska-Bartkowiak, G. Dudziak, R. Sikorski, R. Gras, R. Radhakrishnan, and K. E. Gubbins, J. Chem. Phys. **114**, 950 (2001).
[35] R. J. M. Pellenq and P. E. Levitz, Mol. Phys. **100**, 2059 (2002).
[36] B. Coasne, A. Galarneau, F. Di Renzo, and R. J. M. Pellenq, J. Phys. Chem. C **111**, 15759 (2007).
[37] B. Coasne, A. Galarneau, F. Di Renzo, and R. J. M. Pellenq, Langmuir **22**, 11097 (2006).
[38] B. Coasne, F. Di Renzo, A. Galarneau, and R. J. M. Pellenq, Langmuir **24**, 7285 (2008).
[39] B. Coasne, F. R. Hung, R. J.-M. Pellenq, F. R. Siperstein, and K. E. Gubbins, Langmuir **22**, 194 (2006).
[40] D. Nicholson and N. G. Parsonage, *Computer Simulation and the Statistical Mechanics of Adsorption* (Academic, London, 1982).
[41] M. P. Allen and D. J. Tildesley, *Computer Simulation of Liquids* (Clarendon, Oxford, 1987).
[42] D. Frenkel and B. Smit, *Understanding Molecular Simulation*, 2nd ed. (Academic, New York, 2002).
[43] Q. L. Yan and J. J. de Pablo, J. Chem. Phys. **111**, 9509 (1999).
[44] R. Faller, Q. L. Yan, and J. J. de Pablo, J. Chem. Phys. **116**, 5419 (2002).
[45] E. Marinari and G. Parisi, Europhys. Lett. **19**, 451 (1992).
[46] Q. L. Yan and J. J. de Pablo, J. Chem. Phys. **113**, 1276 (2000).
[47] M. Sliwinska-Bartkowiak, F. R. Hung, E. E. Santiso, B. Coasne, G. Dudziak, F. Siperstein, and K. E. Gubbins, Adsorption **11**, 391 (2005).
[48] F. R. Hung, B. Coasne, K. E. Gubbins, E. E. Santiso, F. R. Siperstein, and M. Sliwinska-Bartkowiak, J. Chem. Phys. **122**, 144706 (2005).
[49] J. S. Rowlinson, *Liquids and Liquid Mixtures* (Butterworth Scientific, London, 1982).
[50] R. J. M. Pellenq and D. Nicholson, J. Phys. Chem. **98**, 13339 (1994).
[51] R. J. M. Pellenq and D. Nicholson, Langmuir **11**, 1626 (1995).
[52] R. Radhakrishnan and K. E. Gubbins, Mol. Phys. **96**, 1249 (1999).
[53] F. R. Hung, G. Dudziak, M. Sliwinska-Bartkowiak, and K. E. Gubbins, Mol. Phys. **102**, 223 (2004).
[54] B. Kuchta, L. Firlej, R. Denoyel, S. Rols, M. R. Johnson, and B. Coasne, J. Chem. Phys. **128**, 184703 (2008).
[55] B. Coasne, C. Alba-Simionesco, F. Audonnet, G. Dosseh, and K. E. Gubbins, Adsorption **13**, 485 (2007).
[56] B. Coasne, C. Alba-Simionesco, F. Audonnet, G. Dosseh, and K. E. Gubbins, Langmuir **25**, 10648 (2009).
[57] P. R. ten Wolde, M. J. Ruiz-Montero, and D. Frenkel, J. Chem. Phys. **104**, 9932 (1996).
[58] B. Coasne, S. K. Jain, and K. E. Gubbins, Phys. Rev. Lett. **97**, 105702 (2006).
[59] B. Coasne, S. K. Jain, L. Naamar, and K. E. Gubbins, Phys. Rev. B **76**, 085416 (2007).
[60] J. Czwartos, M. Sliwinska-Bartkowiak, B. Coasne, and K. E. Gubbins, Pure Appl. Chem. **81**, 1953 (2009).
[61] M. Miyahara, H. Kanda, M. Shibao, and K. Higashitani, J. Chem. Phys. **112**, 9909 (2000).
[62] H. Kanda, M. Miyahara, and K. Higashitani, J. Chem. Phys. **120**, 6173

(2004).
[63] H. Kanda, M. Miyahara, and K. Higashitani, Adsorption **11**, 295 (2005).
[64] K. Koga, G. T. Gao, H. Tanaka, and X. C. Zeng, Nature (London) **412**, 802 (2001).
[65] D. Takaiwa, I. Hatano, K. Koga, and H. Tanaka, Proc. Natl. Acad. Sci. U.S.A. **105**, 39 (2008).
[66] B. Coasne, J. Czwartos, M. Sliwinska-Bartkowiak, and K. E. Gubbins, J. Phys. Chem. B **113**, 13874 (2009).
[67] S. Bhattacharya, B. Coasne, F. R. Hung, and K. E. Gubbins, Langmuir **25**, 5802 (2009).